Field Ionization and Field Emission with Intense, Single-cycle THz Pulses
Need to replace with my own title

by

© Yunxiao Wang

A thesis submitted to the

School of Graduate Studies

in partial fulfilment of the

requirements for the degree of

Anqing, Anhui, China

B.S. in Physics University of Science and Technology of China May 2009

Memorial University of Newfoundland

Doctor of Philosophy

St. John's Newfoundland

Department of Physics August, 2016

Abstract

Nuclear-polarized ^{3}He targets have been widely used in electron-scattering experiments in Thomas Jefferson National Accelerator Facility (JLAB) since mid 1990s. It is of great importance to produce large amounts of ^{3}He gas with high polarization.

The latest experiments run in JLAB prior to the 12GeV upgrade have been using cells polarized with Spin-Exchange Optical Pumping (SEOP). These cells were made of the GE180 glass and use a two-chambered design. The top chamber, known as the pumping chamber, is where ^{3}He is polarized through SEOP. The bottom chamber, known as the target chamber, is where electron scattering occurs. Great effort has been made in our lab to develop this generation of cells. Alkali-hybrid SEOP together with narrowband laser diode arrays have increased the ^{3}He polarization from 37% to 65%. Among other things, we also carefully studied an additional spin relaxation mechanism that limits the maximum achievable ^{3}He polarization.

The 12GeV upgrade makes the future experiments much more demanding in terms of target cell performance. One challenge it brings is the high relaxation due to electron beam. We have designed and tested a new style cell that uses convection instead of diffusion to increase the rate at which the polarization in the target chamber is being replenished by gas from pumping chamber. We have obtained over 50% polarization with controllable convection speed so far.

An additional problem that comes with higher beam current is that the glass end windows of traditional design are not likely to survive the experiments. Our group started exploring the option of using metal end windows from a decade ago. The first problem to solve is to find out the correct material and the proper technique

to incorporate metal without introducing significant spin relaxation and still being able to hold high pressure gas (12 atm) inside. This is a brand new technique that may have a profound impact of future cell designs once fully developed. Although no metal end windows have been tested so far, multiple glass cells with different kinds metal tubes (much larger in area compared to the end windows that will be used in JLAB experiments) attached were examined and were enough to convince us the extra spin relaxation is not likely to cause significant problems. The metals tubes were connected to Pyrex glass with knife-edge (housekeeper) seals and stayed intact through high pressure tests. After exploring options such as pure copper, gold coated copper, titanium, stainless steel, gold coated titanium, we have established that electroplating gold on copper substrate yields the best result so far. Further tests are planned before attaching metal end windows to GE180 glass and using them in electron-scattering experiments.

Acknowledgements

Put your acknowledgements here...

"Intellectual and practical assistance, advice, encouragement and sources of monetary support should be acknowledged. It is appropriate to acknowledge the prior publication of any material included in the thesis either in this section or in the introductory chapter of the thesis."

— MUN School of Graduate Studies

Contents

List of Tables

List of Figures

Chapter 1

Spin-Exchange Optical Pumping

1.1 Overview

Spin-polarized noble gases have been widely used for various purposes [7, 6, 43, 40]. In JLAB (Thomas Jefferson National Accelerator Facility), polarized ^{3}He is used as target for electron-scattering experiments. This is because a ^{3}He nucleus has a pair of protons with paired spins and a single neutron that contributes the most of the nuclear spin. In MRI, polarized ^{3}He has seen uses such as detecting structural damage in the lungs.

There are generally two ways of polarizing ^{3}He: Metastability-Exchange Optical Pumping (MEOP) [23] and Spin-Exchange Optical Pumping (SEOP) [22, 36, 39]. Our group focuses on SEOP as MEOP polarizes gas at relatively low pressure ($\sim$1 torr), thus further compression is required to produce target cells of several atms that meet the need of JLab experiments.

In SEOP, alkali metal is polarized by circularly polarized laser light tuned to the

D1 transition of the particular alkali species used. ^{3}He obtains polarization from alkali metal through spin-exchange process [15]. With the combination of hybrid alkali mixtures (typically Rb and K) and spectrally narrowed lasers [31, 10], more than 80% polarizations have been produced.

1.2 Optical pumping

1.2.1 Rb for SEOP

In optical pumping, Rb is often the alkali metal chosen to be optically pumped by circularly polarized laser light. The angular momentum of polarized photons are transfered to the valence electrons of Rb atoms[55]. Sometimes hybrid mixtures of Rb and K are used together, in which case Rb is still the alkali metal that is directly pumped by laser light while K serves as an efficient medium to transfer the polarization from Rb to ^{3}He. Because the spin destruction rates are much lower for lighter alkali metals, K-^{3}He spin-exchange process is a lot more efficient than that of Rb-^{3}He. Rb is still selected as the alkali metal to be pumped directly because of the relative ease of acquiring laser at the Rb D_1 line wavelength and the wide separation its between D_1 (794.7nm) and D_2 line (780nm).

The Rb melting point is at 39.5°C, so it's easy to achieve enough Rb vapor without having to drive the oven temperature too high. In our lab, depending on if the cell contains pure Rb or Rb/K mixture, the oven temperature can be between 85°C to as high as 255°C. Perhaps the most used oven temperature for hybrid cells is 235°C which has empirically been a good temperature to produce Rb/K mixture vapor,

while around 170°C is typically enough for pure Rb.

1.2.2 Vapor Pressure Curves

When the alkali metal is heated to above its melting point, a small amount of alkali metal atoms evaporate. The equilibrium vapor pressure is temperature dependent:

$$P = 10^{5.006+\alpha+\beta/T}\text{Pa} \tag{1.1}$$

where α and β are listed in Table 1.2.2 [16].

	Patassium	Rubidim
α	4.402	4.312
β	-4453	-4040

Thus the number density is

$$[A] = \frac{10^{5.006+\alpha+\beta/T}}{k_B T} \tag{1.2}$$

The number density curves of pure Rb and K vapor are shown in Fig. 1.1.

1.2.3 Energy Levels of Alkali Metal in External Magnetic Field

The Hamiltonian for ground state (L=0) alkali metal atoms in external magnetic field is:

$$\mathbf{H} = A\mathbf{I}\cdot\mathbf{S} - g_e\mu_B S_z B_z - g_N\mu_N I_z B_z \tag{1.3}$$

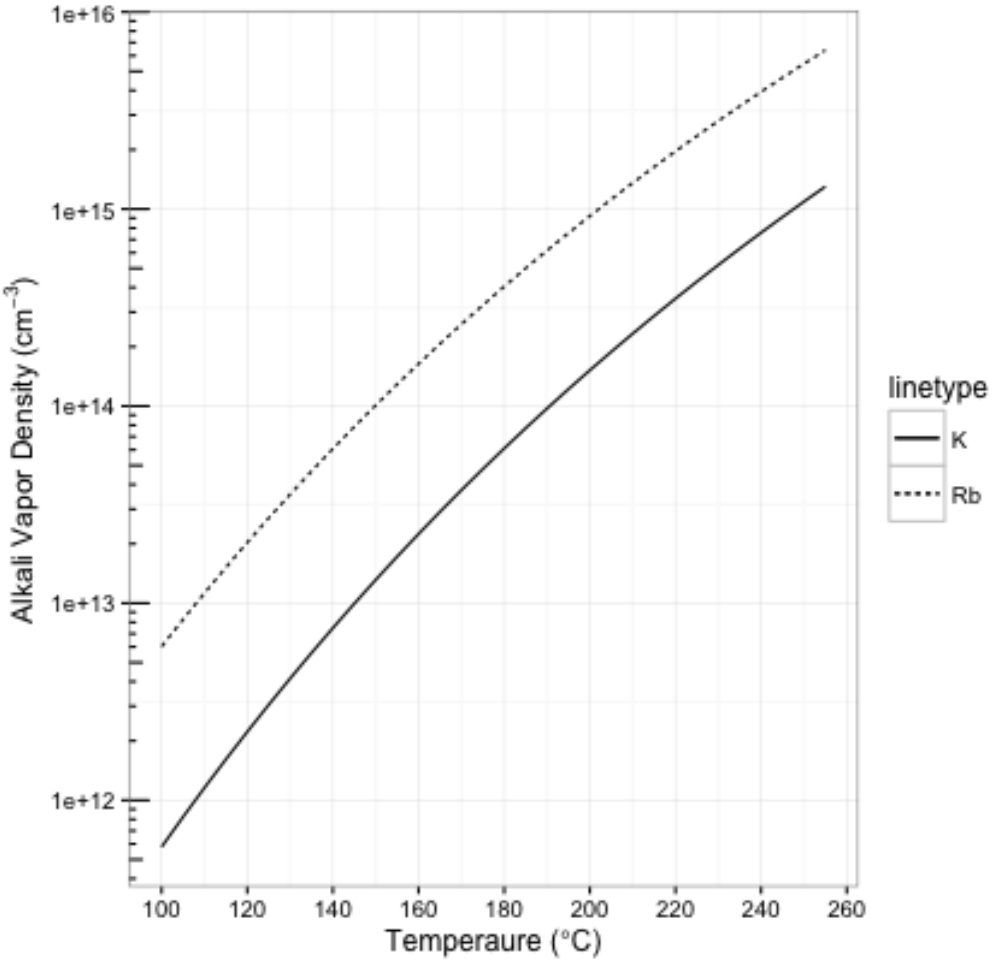

Figure 1.1: Rb And K Number Density Curves

The first term $A\mathbf{I} \cdot \mathbf{S}$ describes the coupling of the nuclear spin $\mathbf{I}$ with the electron spin $\mathbf{S}$ and is key to spin exchange, where A is the isotropic magnetic-dipole coupling coefficient [8]. The resulting energy levels from the first term are referred to as hyperfine structure. The second and third terms describe the Zeeman splitting due to the presence of an external magnetic field. $\mu_B = 9.274 \times 10^{-24}$J/T and $\mu_N = 5.051 \times 10^{-27}$J/T are the Bohr and nuclear magnetons. $g_e \approx 2$ and $g_N \approx 5.59$ are the electronic and nuclear Lande g-factors.

The linear relationship between energy levels and magnetic field only holds for weak magnetic fields which applies to our lab where ∼13 Gauss is used most of the time. When the Zeeman splitting grows comparable to the hyperfine energy difference one would have to take into account the quantum mixing of the states, the result is described by Breit-Rabi Formula. With ∼13 Gauss, the hyperfine term dominates the total Hamiltonian. ^{85}Rb and ^{87}Rb are both present in the alkali metal used for SEOP, the energy levels of ^{87}Rb are shown in Fig. 1.2.

1.2.4 Optical Pumping Process Overview

For simplicity, the following discussion will ignore the nuclear spins for now. The inclusion of nuclear spins will increase the number of energy states but the optical pumping mechanism remains the same. In our typical setup, circularly polarized laser light is tuned to the D1 line of Rb and excites valence electrons of Rb from $5S_{1/2}$ state to $5P_{1/2}$ state as shown in Fig. 1.3[55].

Left-circularly polarized light is assumed in the figure. Conservation of angular momentum requires $\Delta m = +1$ as the figure shows. Through collisions with other Rb atoms, excited electrons will mix and evenly distribute between the two $2P_{1/2}$ states. Electrons then decay to the two ground states with equal probabilities. The selection rule for the decay process is $\Delta m = 0$ or ± 1. Even though both ground states receive electrons from the decay, only the m = -1/2 state absorbs the circular polarized photons and is being depleted, so atoms are in effect pumped to the m = +1/2 state. When we consider Rb with nuclear spins, both $5S_{1/2}$ and $5P_{1/2}$ states are split into more energy levels, but the net effect is still that the ground state with

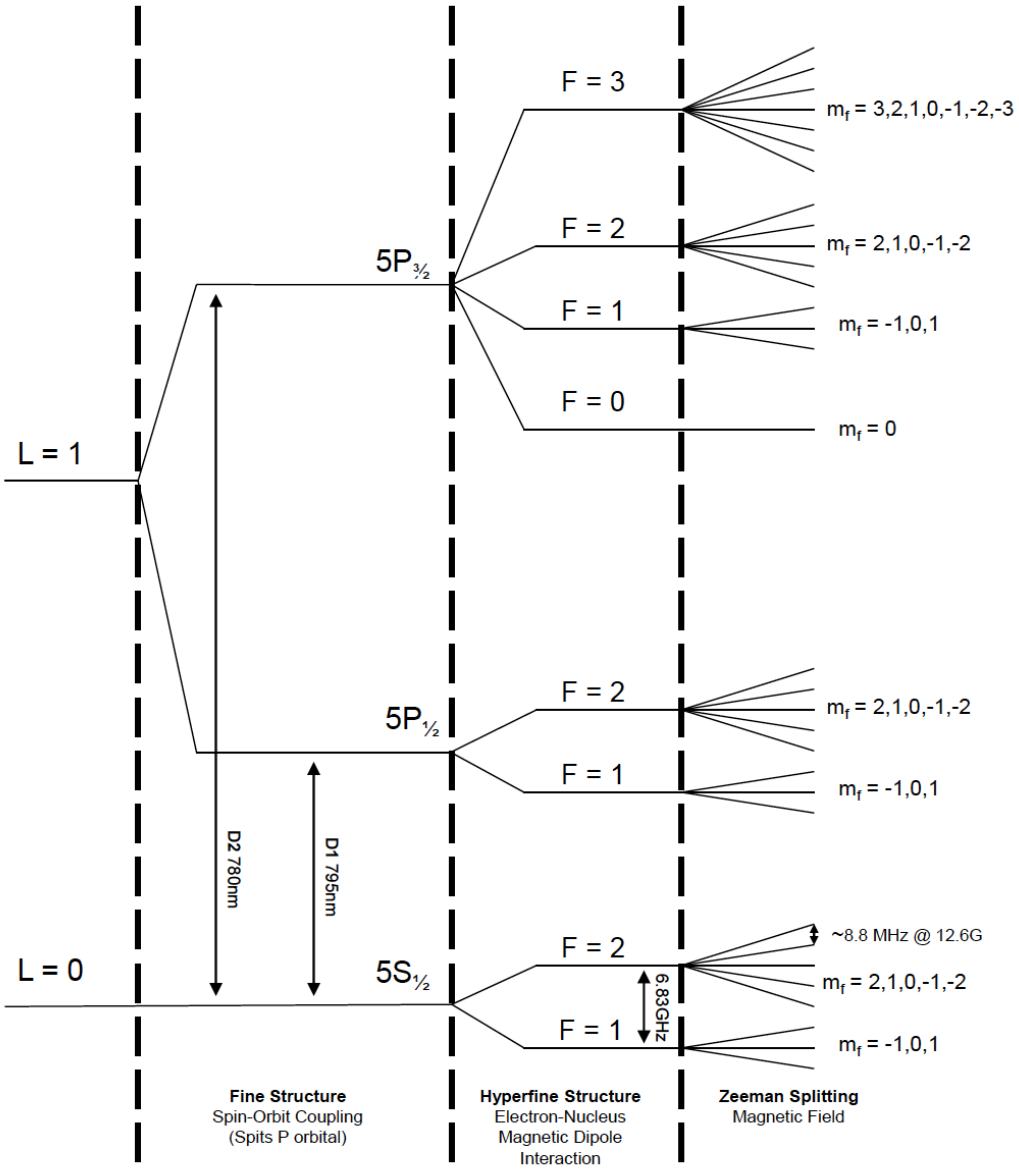

Figure 1.2: Level Diagram of ^{87}Rb. The splittings are not to scale. Adapted from Dolph's PhD thesis.

highest m accumulate atoms over time.

When the excited electrons decay back to the ground state, they emit unpolarized photons with angular momentum in random directions which can depolarize the gas.

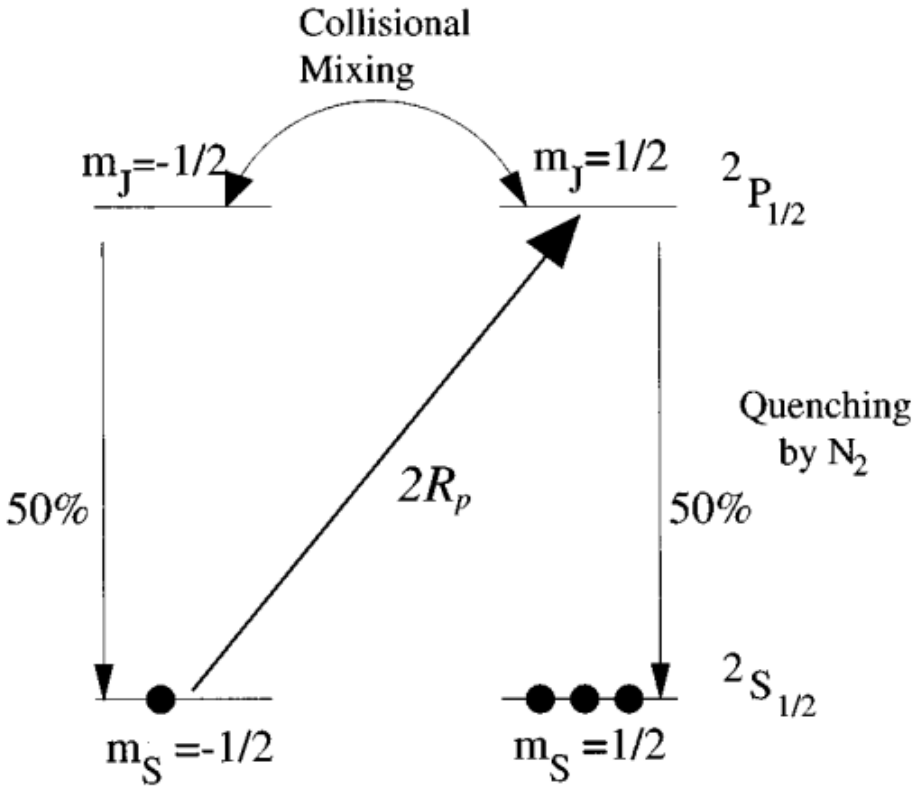

Figure 1.3: The interaction of alkali-metal atoms with left-circularly (σ^+) polarized light. (from Ref. [55])

A small amount of N_2 gas is added into the cell (typically around 0.1 Amagats) to non-radiatively quench the excited electrons as N_2 molecules can absorb the released energy of spontaneous decays into their rotational and vibrational modes of oscillation. With an appropriate amount of N_2[53], the photon-emitting decays can be reduced to less than 3%.

1.2.5 Optical Pumping Rate

The optical pumping rate at position $\vec{r}$ can be described by

Table 1.1: Pressure broadening of Rb D_1 lines by ^{3}He, ^{4}He and N_2. The broadening and shifting density coefficients are listed. The 4th and 6th columns are the temperature dependence for He and N_2, respectively. All coefficients are given for 353 K, values for different temperatures can be calculated with the temperature dependence.

	^{4}He	^{3}He	Temp. depen.	N_2	Temp. depen.
D_1 full width (GHz/amg)	18.0±0.2	18.7±0.3	$T^{0.05\pm0.05}$	17.8±0.3	$T^{0.3}$
D_1 line shift (GHz/amg)	4.3±0.1	5.64±0.15	$T^{1.1\pm0.1}$	-8.25±0.15	$T^{0.3}$

$$R = \int \Phi(\nu, \vec{r})\sigma(\nu)d\nu \tag{1.4}$$

where $\Phi(\nu, \vec{r})$ is the position dependent photon spectral flux density and $\sigma(\nu)$ is the photon absorption cross section. The cross section has a natural Lorentzian lineshape which is broadened by the Doppler effect and pressure broadening. The pressure broadening effect dominates the lineshape as our cells normally have densities well above one amagat. The collisions of Rb with ^{3}He and N_2 cause the broadening as well as a slight frequency shift of the D_1 line. The coefficients of pressure broadening for ^{3}He, ^{4}He and N_2 are listed in Table 1.1, and can be used to calculate the broadened line width and the shifted line center.

$\sigma(\nu)$ follows the sum rule[38]:

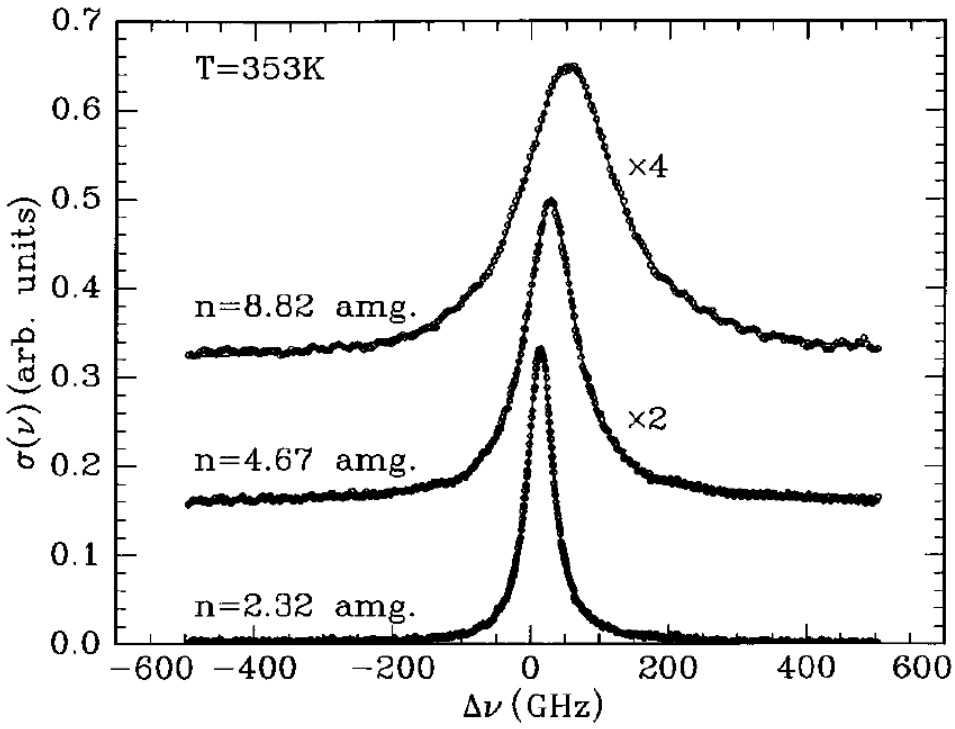

Figure 1.4: Absorption cross section for Rb D_1 line in the presence of three different densities of ^{3}He. (from Ref. [45])

$$\int \sigma(\nu) d\nu = \pi r_0 c f \tag{1.5}$$

where $r_0 = 2.82 \times 10^{-13}$ cm is the classical electron radius and $f = 0.337$ [36] is the transition oscillator strength. Since our lineshape is dominated by pressure broadening, the photon absorption cross section is well approximated by a Lorentzian lineshape:

$$\sigma(\nu) = f r_e c \frac{\frac{\Gamma_A}{2}}{(\nu - \nu_0)^2 + (\frac{\Gamma_A}{2})^2} \tag{1.6}$$

where Γ_A is the pressure dependent FWHM, $\Gamma_A \approx 0.04$nm/amg$\cdot$ [^{3}He]. At the front

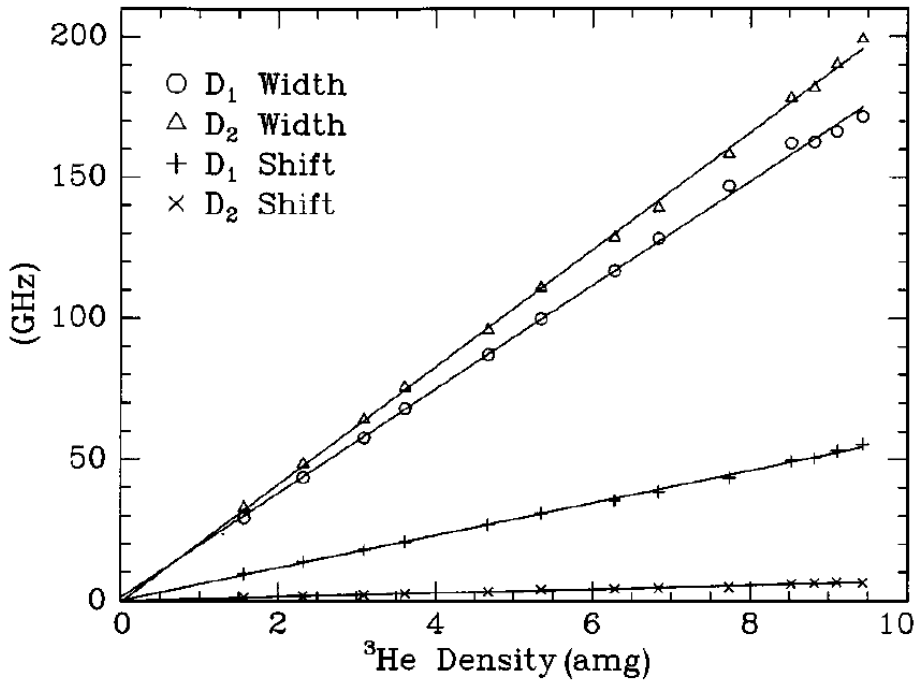

Figure 1.5: The shift and the broadening due to presence of ^{3}He for Rb D_1 and D_2 lines. (from Ref. [45])

of the cell, the photon spectral flux density is reasonably described as the product of a Gaussian spatial distribution and a Gaussian spectrum.

$$\phi(\nu, \vec{r}) = \phi_0(\vec{r})G(\nu) \tag{1.7}$$

with

$$\phi_0(\vec{r}) = \frac{P}{h\nu}\frac{2}{\omega^2\pi}e^{2r^2/\omega^2} \tag{1.8a}$$

$$G(\nu) = \frac{1}{\sqrt{2\pi}\sigma_l}e^{-(\nu-\nu_l)^2/2\sigma_l^2} \tag{1.8b}$$

where P is the laser power; ω is the beam waist; σ_l is the Gaussian width of the laser and ν_l is the central laser frequency.

1.2.6 Polarization Time Evolution

^{3}He nuclei have an intrinsic nuclear spin of 1/2, thus it is relatively simple to explain the math of polarization accumulation with ^{3}He as the example. One typically defines the polarization as the asymmetry between +1/2 state and -1/2 state:

$$P = \frac{\rho_{+1/2} - \rho_{-1/2}}{\rho_{+1/2} + \rho_{-1/2}} = \rho_{+1/2} - \rho_{-1/2} \tag{1.9}$$

where $\rho_{\pm 1/2}$ is the ensemble population in the $\pm 1/2$ state.

While it might not be true for Rb, we are only treating the time evolution of polarization of Rb electrons the same as ^{3}He for our purpose with the following the equation:

$$\frac{dP}{dt} = \gamma(1 - P) - \Gamma \cdot P \tag{1.10}$$

where γ is the polarization rate and Γ is the depolarization rate due to all other processes. The solution of this differential equation has the simple form of:

$$P(t) = Ce^{-(\gamma+\Gamma)t} + \frac{\gamma}{\gamma + \Gamma} \tag{1.11}$$

The saturated polarization is defined as the value of P in the limit t $\to \infty$:

$$P_\infty = \frac{\gamma}{\gamma + \Gamma} \tag{1.12}$$

The initial polarization is defined as the value of P at t = 0:

$$P_0 = C + \frac{\gamma}{\gamma + \Gamma} = C + P_\infty \tag{1.13}$$

Thus, P(t) can be expressed as:

$$P(t) = (P_0 - P_\infty)e^{-(\gamma+\Gamma)t} + P_\infty \tag{1.14}$$

In the case of polarizing Rb with a pump laser, γ is the pumping rate R and Γ is the Rb spin relaxation rate Γ_{Rb}. There is typically a small angle θ between the pump laser and the holding field even though great effort has been made to minimize the angle. Thus P(t) can be rewritten as:

$$P(t) = P_0 e^{-(R+\Gamma_{Rb})t} + P_{laser} cos\theta \frac{R}{R+\Gamma_{Rb}}(1 - e^{-(R+\Gamma_{Rb})t}) \tag{1.15}$$

where θ is called the skew angle, P_{laser} is the circular polarization of the pump laser which is normally above 99.5%. Rb close to the front side of the cell can reach above 97% (depends on the laser power and other factors) on the order of 100's of microseconds. As the laser propagates through the cell, power is attenuated by Rb vapor. Therefore Rb polarization at the back side of the cell is typically lower than that at the front side. One way to minimize this problem is to shine pump laser light from both sides of the cell to achieve higher overall Rb polarization and ^{3}He polarization.

Spins are thermally polarized in the presence of a magnetic field even without being actively polarized. The probability for a spin to be in state s is:

$$Prob. = \frac{e^{-E_s/k_B T}}{\sum_{si} e^{-E_{si}/k_B T}} \tag{1.16}$$

where E_s is the energy of the state, k_B is the Boltzmann constant and T is the temperature. Using the thermal distribution, under typical operating conditions,

^3He polarization is 10^{-9} and Rb polarization is 10^{-5}. Both are negligible without active pumping.

1.2.7 Rb Spin Destruction Rate

There are two main mechanisms of Rb depolarization: the binary collisions with Rb, ^{3}He and N_2, and the formation and breakup of van der Waals molecules, the second mechanism is negligible for ^{3}He cells [55]. The Rb spin destruction rate can then be expressed as

$$\Gamma_{Rb} = k_{Rb-Rb}[Rb] + k_{Rb-^3He}[^3He] + k_{Rb-N_2}[N_2] \tag{1.17}$$

where k_{Rb-X} is the spin destruction rate constant and [X] is the density of X. The constants are listed as follows [54, 46]:

$$k_{Rb-^3He}(T) = 55.9(9)\left(\frac{T}{473.15K}\right)^{3.31(12)} \text{Hz/amg} \tag{1.18a}$$

$$k_{Rb-N_2}(T) = 290(30)\left(\frac{T}{473.15K}\right)^{2.0(25)} \text{Hz/amg} \tag{1.18b}$$

$$k_{Rb-Rb} = 4.813(48) \times 10^{-13}\text{Hz} \cdot \text{cm}^3 \tag{1.18c}$$

For a pure Rb cell at 170°C with the following densities in the pumping chamber:

$$[^3He] \approx 8.0\text{amg} \tag{1.19a}$$

$$[N_2] \approx 0.08\text{amg} \tag{1.19b}$$

$$[Rb] \approx 6.0 \times 10^{14}\text{cm}^{-3} \tag{1.19c}$$

The approximate spin destruction rates due to various gases are:

$$\Gamma_{Rb-^3He} \approx 360Hz \tag{1.20a}$$

$$\Gamma_{Rb-N_2} \approx 20Hz \tag{1.20b}$$

$$\Gamma_{Rb-Rb} \approx 289Hz \tag{1.20c}$$

The total spin destruction rate is 669 Hz. By contrast, the average optical pumping rate at the front of the cell with 20 W and 1.5 cm beam radius narrowband laser light is often of 100s kHz.

1.3 Spin Exchange

Following equation 1.15, the time evolution of ^3He polarization can be expressed as:

$$P_{^3He}(t) = P_0 e^{-(\gamma_{se}+\Gamma)t} + P_{Rb}\frac{\gamma_{se}}{\gamma_{se}+\Gamma}(1 - e^{-(\gamma_{se}+\Gamma)t}) \tag{1.21}$$

The saturation polarization is

$$P_\infty = P_{Rb}\frac{\gamma_{se}}{\gamma_{se}+\Gamma} \tag{1.22}$$

where γ_{se} is the spin exchange rate between ^{3}He and Rb, and Γ is the spin relaxation rate.

1.3.1 Spin-Dependent Interactions

The key process in spin-exchange optical pumping is collisional transfer of polarization between optically pumped alkali-metal atoms and the nuclei of the noble gas atoms.

As in Fig. 1.6, the transfer of angular momentum occurs either while the atoms are bound in van der Waals molecules or in simple binary collisions. The first mechanism is only important for heavy noble gas nuclei such as X3, while binary collisions is the dominating mechanism for ^{3}He. The time scale for binary collisions is on the order of 10^{-12} sec, the collision can induce both $\Delta F = \pm 1$ and $\Delta F = 0$ transitions between hyperfine sublevels. For heavier noble gases like ^{129}Xe at pressure of a few tens of Torr, the contributions of van der Waals molecules can greatly exceed that of binary collisions. At several atms which is the typical operating pressure for SEOP, the time scale of van der Waals molecules is greatly limited by collision so that the binary collisions dominate [55].

Spin-dependent interactions produce the spin transfer and relaxation. For SEOP, spin-rotation interaction between $\vec{S}$ and the rotational angular momentum $\vec{N}$ of the atom pair formed by Rb and noble gas atom, and the isotropic hyperfine interaction between $\vec{S}$ and the noble-gas nuclear spin $\vec{I}_b$ dominate the spin-exchange process:

$$V_1(\vec{R}) = \gamma(R)\vec{N} \cdot \vec{S} + A(R)\vec{I}_b \cdot \vec{S} \tag{1.23}$$

The spin-rotation interaction is caused by the magnetic fields from relative motion of the charges of the colliding atoms, and the isotropic hyperfine interaction originates from the Fermi-contact magnetic fields produced by two nuclei. The spin-rotation interaction produces relaxation of the alkali-metal electron-spins, while the isotropic hyperfine interaction transfers angular momentum back and forth between the alkali-metal electron spins and the noble-gas nuclear spins.

An alkali-metal atom and a noble-gas atom interact via both a large spin-independent

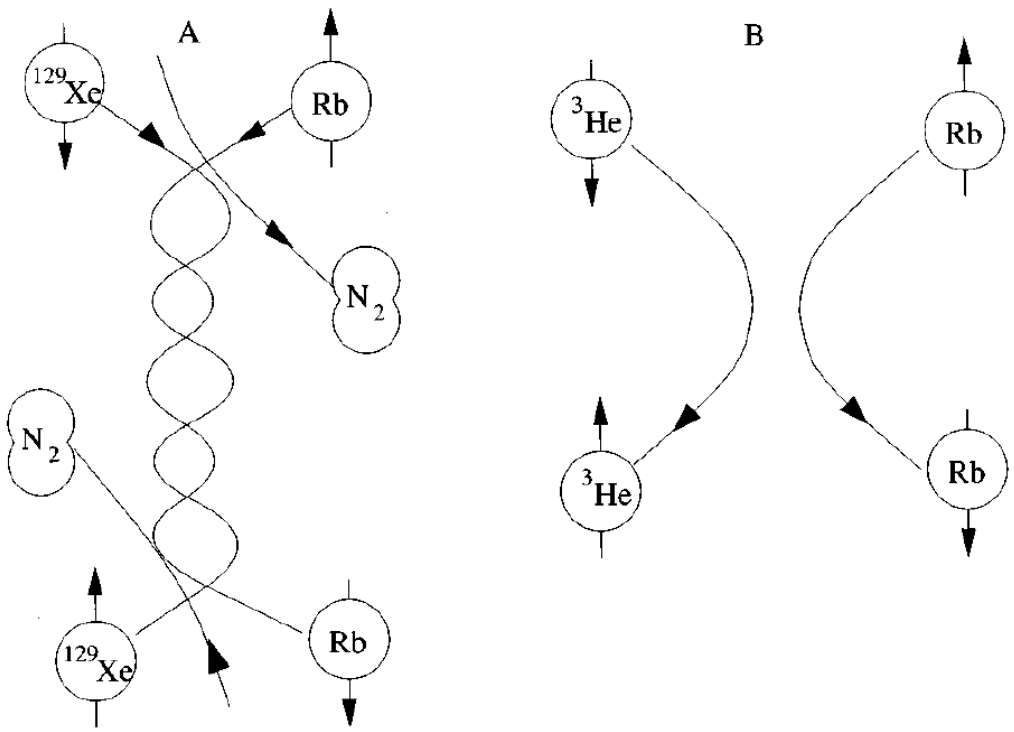

Figure 1.6: A. Formation and breakup of alkali-metal/noble-gas van der Waals molecule. B. Binary collision between an alkali-metal atom and a noble-gas atom. (from Ref. [55])

interaction $V_0(R)$ and a small spin-dependent interaction $V_1(R)$. At the high operating temperatures, V_0 determines classical collision trajectories, while V_1 acts as a small perturbation. We'll focus on V_1 below since it is responsible for spin exchange.

Including a few more terms that were neglected in Eq. 1.23, the spin-dependent interaction $V_1(R)$ can be expressed as [55]:

$$V_1(\vec{R}) = \gamma(R)\vec{N}\cdot\vec{S} + \sum_k A_k(R)\vec{I}_k\cdot\vec{S} + \sum_k B_k(R)\vec{I}_k\cdot(3\vec{R}\vec{R}-1)\cdot\vec{S} + \sum_k C_k(R)\vec{I}_k\cdot(3\vec{R}\vec{R}-1)\cdot\vec{I}_k \tag{1.24}$$

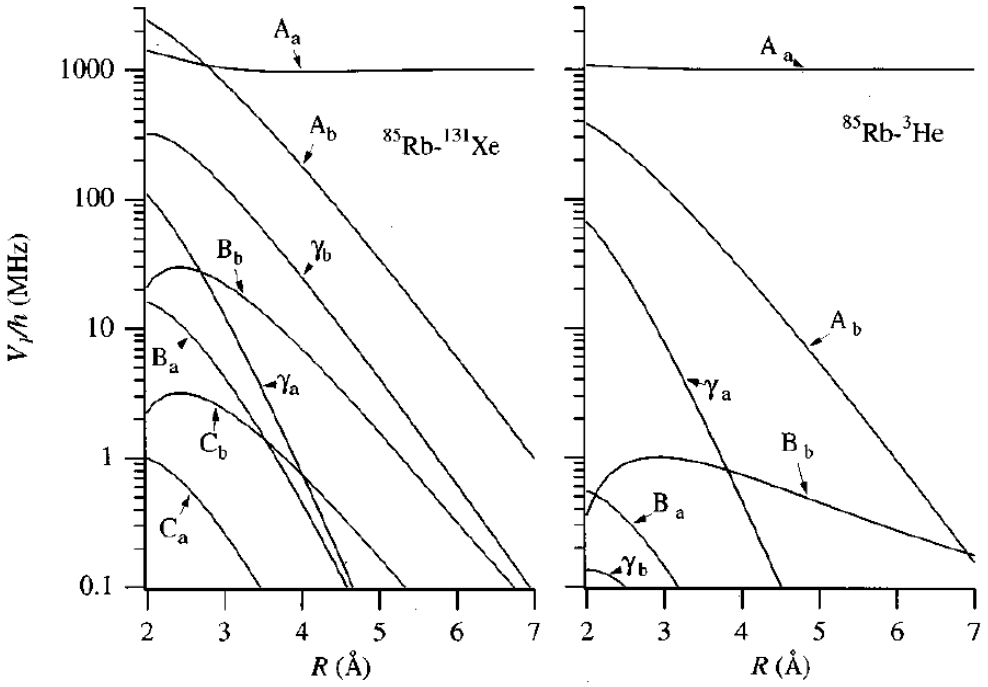

Figure 1.7: Strengths of various spin-dependent interactions as functions of separation(from Ref. [55])

where $\vec{I}_a$ and $\vec{I}_b$ are the nuclear spins of the atomic pair, where a stands for alkali metal atom and b stands for noble gas atom. γ is the coefficient of the spin-rotation interaction, while A_k, B_k, C_k are the coefficients for isotropic magnetic-

dipole hyperfine interactions, anisotropic magnetic-dipole hyperfine interactions, and electric quadrupole interactions, respectively. A_a greatly exceed other coefficients as the separations between atoms increase.

The isotropic hyperfine interactions come from the Fermi-contact magnetic fields of the two nuclei. A_b is the term responsible for spin exchange:

$$A_b(R) = \frac{8\pi g_s \mu_B \mu_b}{3I_b} |\eta\phi_0(R)|^2 \tag{1.25}$$

where η is the enhancement factor which equals to the ratio of the perturbed wave function at the noble gas nucleus to that without the noble gas atom. The isotropic hyperfine interaction also introduces a frequency shift of the magnetic resonance lines for alkali-metal and noble gas atoms. The frequency shift is characterized by another enhancement factor κ which is the ratio of the actual shift of the alkali metal electron lines due to the presence of polarized noble gas nuclei to what would be produced by the bulk magnetization of polarized noble gas. The shift is used in the technique Electron Paramagnetic Resonance (EPR) to calculate the polarization of noble gas nuclei.

The isotropic magnetic-dipole coupling polarizes the noble gas nuclei parallel to the electron spin polarization, while the anisotropic magnetic-dipole coupling polarizes in the opposite direction. Even though the anisotropic magnetic-dipole coupling is weak compared with the isotropic interaction, it might be an important factor for the "X factor" that will be discussed later.

1.3.2 Spin Exchange Rate

The spin exchange rate due to binary collisions is:

$$\gamma_{se} =< \sigma_{se} v > [Rb] = k_{se}[Rb] \tag{1.26}$$

where $k_{se} =< \sigma_{se} v >$ is the velocity-averaged spin exchange rate constant. k_{se} for spin exchange between ^{3}He and Rb is [13]:

$$k_{se}^{^3He-Rb} = (6.7 \pm 0.7) \times 10^{-20} cm^3/s \tag{1.27}$$

At 170°C which is a typical temperature that we run tests with,

$$[Rb] = 2.60 \times 10^{14} cm^{-3} \tag{1.28}$$

Thus for a simple spherical cell with pure Rb,

$$\frac{1}{\gamma_{se}} \approx 15.9 hrs \tag{1.29}$$

1.4 ^{3}He Spinup and Relaxation

Similar to the optical pumping process of Rb, ^3He polarization can be described by

$$P_{^3He}(t) = P_0^{^3He} e^{-(\gamma_{se}+\Gamma)t} + P_\infty^{^3He}(1 - e^{-(\gamma_{se}+\Gamma)t}) \tag{1.30}$$

where the saturation polarization is

$$P_\infty^{^3He} = P_\infty^{Rb} \frac{\gamma_{se}}{\gamma_{se} + \Gamma} \tag{1.31}$$

And Γ is the total relaxation rate of ^{3}He nucleus spin polarization due to all processes except for spin exchange,

$$\Gamma = \Gamma_{dipolar} + \Gamma_{inhomogeneity} + \Gamma_{wall} \tag{1.32}$$

When a target cell are used in electron scattering experiments where an electron beam goes through part of the cell, an additional relaxation rate due to the beam Γ_{beam} should also be included.

The coupling of nuclear spin to orbital angular momentum creates an intrinsic ^{3}He relaxation rate that depends on density. At room temperature ($23°C$), the dipolar relaxation rate is [39]

$$\frac{1}{\Gamma_{dipolar}} = \frac{[^3He]}{744} hr^{-1} \tag{1.33}$$

where $[^3He]$ is the ^3He density in amagats. Assuming the cell density is 8 amg, the relaxation rate is $1/93\ hr^{-1}$. In addition, there is an additional intrinsic relaxation due to the spin-rotation interaction. This mechanism dominates the relaxation for ^{129}Xe but is small for ^{3}He.

The relaxation rate due to field inhomogeneities is [29, 47, 19]

$$\Gamma_{inhomogeneity} = D\frac{|\nabla B_x|^2 + |\nabla B_y|^2}{B_0^2} \tag{1.34}$$

where D is the ^{3}He diffusion constant, ∇B_x and ∇B_y are the transverse magnetic field inhomogeneities, B_0 is the holding field along z-axis. Under operating conditions, assuming the pressure is around 12 atm and field is 12.6 G, $D \approx 0.16 cm^2/s$ and the field inhomogeneities are 10mG/cm, the relaxation rate is $1/1400$ hr^{-1}.

Wall relaxation is typically the dominant relaxation mechanism for cells in our lab. This mechanism depends on the properties of the inner surface of glass. Most of the target cells are contructed with reblown General Electric Type 180 (GE-180) glass. This aluminosilicate glass is highly impermeable to ^{3}He. The wall relaxation is believed to be associated to several different mechanisms, such as paramagnetic impurities in the glass and microfissures in the surface that could trap ^{3}He atoms. It has been found reblowing the glass can help lower the wall relaxation rate because it reduces the number of microfissures. The wall relaxation is not well understood, but it is believed to scale with the surface-to-volume ratio:

$$\Gamma_{wall} = \rho S/V \tag{1.35}$$

where ρ is called relaxivity.

1.5 X Factor

In 2006, Babcok *et al.* reported evidence of a previously unrecognized spin relaxation mechanism, and named it X factor. This mechanism appears to be temperature dependent and roughly proportional to alkali density. The X factor limits the maximally achievable ^{3}He polarization even with infinite laser power. The saturation polarization is

$$P_\infty^{^3He} = P_\infty^{Rb} \frac{\gamma_{se}}{\gamma_{se}(1+X)+\Gamma} \tag{1.36}$$

In the presence of infinite laser power where $\gamma_{se} \gg \Gamma$, the saturation polarization becomes

$$P_{\infty}^{^3He} = P_{\infty}^{Rb}\frac{1}{1+X} \tag{1.37}$$

The X factor will be discussed in greater detail in chapter 4.

Bibliography

[1] Nuclear relaxation of ^{3}he gas on various solid surfaces. *Canadian Journal of Physics*, 1971.

[2] Physics of practical spin-exchange optical pumping. *PhD thesis, University of Wisconsin-Madison*, 2001.

[3] Alkali-hybrid spin-exchange optically-pumped polarized ^{3}he targets used for studying neutron structure. *PhD thesis, University of Virginia*, 2010.

[4] High-performance nuclear-polarized ^{3}He targets for electron scattering based on spin-exchange optical pumping. *PhD thesis, University of Virginia*, 2010.

[5] A. Abragam. *Principles of Nuclear Magnetism.*

[6] M. Amarian, L. Auerbach, T. Averett, J. Berthot, P. Bertin, W. Bertozzi, T. Black, E. Brash, D. Brown, E. Burtin, J. R. Calarco, G. D. Cates, Z. Chai, J.-P. Chen, S. Choi, E. Chudakov, E. Cisbani, C. W. de Jager, A. Deur, R. DiSalvo, S. Dieterich, P. Djawotho, M. Finn, K. Fissum, H. Fonvieille, S. Frullani, H. Gao, J. Gao, F. Garibaldi, A. Gasparian, S. Gilad, R. Gilman, A. Glamazdin, C. Glashausser, E. Goldberg, J. Gomez, V. Gorbenko, J.-O. Hansen, F. W.

Hersman, R. Holmes, G. M. Huber, E. W. Hughes, T. B. Humensky, S. Incerti, M. Iodice, S. Jensen, X. Jiang, C. Jones, G. M. Jones, M. Jones, C. Jutier, A. Ketikyan, I. Kominis, W. Korsch, K. Kramer, K. S. Kumar, G. Kumbartzki, M. Kuss, E. Lakuriqi, G. Laveissiere, J. Lerose, M. Liang, N. Liyanage, G. Lolos, S. Malov, J. Marroncle, K. McCormick, R. McKeown, Z.-E. Meziani, R. Michaels, J. Mitchell, Z. Papandreou, T. Pavlin, G. G. Petratos, D. Pripstein, D. Prout, R. Ransome, Y. Roblin, D. Rowntree, M. Rvachev, F. Sabatie, A. Saha, K. Slifer, P. A. Souder, T. Saito, S. Strauch, R. Suleiman, K. Takahashi, S. Teijiro, L. Todor, H. Tsubota, H. Ueno, G. Urciuoli, R. Van der Meer, P. Vernin, H. Voskanian, B. Wojtsekhowski, F. Xiong, W. Xu, J.-C. Yang, B. Zhang, and P. Zolnierczuk. Q^2 evolution of the generalized gerasimov-drell-hearn integral for the neutron using a ^{3}He target. *Phys. Rev. Lett.*, 89:242301, Nov 2002.

[7] P. L. Anthony, R. G. Arnold, H. R. Band, H. Borel, P. E. Bosted, V. Breton, G. D. Cates, T. E. Chupp, F. S. Dietrich, J. Dunne, R. Erbacher, J. Fellbaum, H. Fonvieille, R. Gearhart, R. Holmes, E. W. Hughes, J. R. Johnson, D. Kawall, C. Keppel, S. E. Kuhn, R. M. Lombard-Nelsen, J. Marroncle, T. Maruyama, W. Meyer, Z.-E. Meziani, H. Middleton, J. Morgenstern, N. R. Newbury, G. G. Petratos, R. Pitthan, R. Prepost, Y. Roblin, S. E. Rock, S. H. Rokni, G. Shapiro, T. Smith, P. A. Souder, M. Spengos, F. Staley, L. M. Stuart, Z. M. Szalata, Y. Terrien, A. K. Thompson, J. L. White, M. Woods, J. Xu, C. C. Young, and G. Zapalac. Determination of the neutron spin structure function. *Phys. Rev. Lett.*, 71:959–962, Aug 1993.

[8] S. Appelt, A. B.-A. Baranga, C. J. Erickson, M. V. Romalis, A. R. Young, and

W. Happer. Theory of spin-exchange optical pumping of ^{3}He and ^{129}Xe. *Phys. Rev. A*, 58:1412–1439, Aug 1998.

[9] E. Babcock, B. Chann, T. G. Walker, W. C. Chen, and T. R. Gentile. Limits to the polarization for spin-exchange optical pumping of ^{3}He. *Phys. Rev. Lett.*, 96:083003, Mar 2006.

[10] E. Babcock, I. Nelson, S. Kadlecek, B. Driehuys, L. W. Anderson, F. W. Hersman, and T. G. Walker. Hybrid spin-exchange optical pumping of ^{3}He. *Phys. Rev. Lett.*, 91:123003, Sep 2003.

[11] E. Babcock, I. A. Nelson, S. Kadlecek, and T. G. Walker. ^{3}He polarization-dependent epr frequency shifts of alkali-metal$^{\smile}$^{3}He pairs. *Phys. Rev. A*, 71:013414, Jan 2005.

[12] R. M. Barrer. *Diffusion in and through Solids.*

[13] A. Ben-Amar Baranga, S. Appelt, M. V. Romalis, C. J. Erickson, A. R. Young, G. D. Cates, and W. Happer. Polarization of ^{3}He by spin exchange with optically pumped rb and k vapors. *Phys. Rev. Lett.*, 80:2801–2804, Mar 1998.

[14] F. Bloch. Nuclear induction. *Phys. Rev.*, 70:460–474, Oct 1946.

[15] M. A. Bouchiat, T. R. Carver, and C. M. Varnum. Nuclear polarization in he^3 gas induced by optical pumping and dipolar exchange. *Phys. Rev. Lett.*, 5:373–375, Oct 1960.

[16] A. C., V. Itkin, and H. M.K. *Candadian Metallurgial Quarterly*, 23, 1984.

[17] P. Callaghan. *Principles of Nuclear Magnetic Resonance Microscopy.*

[18] G. D. Cates. Polarized targets in high energy physics. *Proceedings of the 1993 Summer Institute on Particle Physics: Spin Structure in High Energy Processes (SSI93)*, SLAC-R-444:185–207, 1993.

[19] G. D. Cates, S. R. Schaefer, and W. Happer. Relaxation of spins due to field inhomogeneities in gaseous samples at low magnetic fields and low pressures. *Phys. Rev. A*, 37:2877–2885, Apr 1988.

[20] G. D. Cates, D. J. White, T.-R. Chien, S. R. Schaefer, and W. Happer. Spin relaxation in gases due to inhomogeneous static and oscillating magnetic fields. *Phys. Rev. A*, 38:5092–5106, Nov 1988.

[21] B. Chann, E. Babcock, L. W. Anderson, and T. G. Walker. Measurements of ^{3}He spin-exchange rates. *Phys. Rev. A*, 66:032703, Sep 2002.

[22] T. E. Chupp, M. E. Wagshul, K. P. Coulter, A. B. McDonald, and W. Happer. Polarized, high-density, gaseous ^{3}He targets. *Phys. Rev. C*, 36:2244–2251, Dec 1987.

[23] F. D. Colegrove, L. D. Schearer, and G. K. Walters. Polarization of he^3 gas by optical pumping. *Phys. Rev.*, 132:2561–2572, Dec 1963.

[24] I. Delstar Metal Finishing. *https://www.delstar.com/electropolishing*.

[25] A. Deninger, W. Heil, W. E. Otten, M. Wolf, K. R. Kremer, and A. Simon. Paramagnetic relaxation of spin polarized 3he at coated glass walls. *The European Physical Journal D - Atomic, Molecular, Optical and Plasma Physics*, 38(3):439–443, 2006.

[26] P. A. M. Dolph, J. Singh, T. Averett, A. Kelleher, K. E. Mooney, V. Nelyubin, W. A. Tobias, B. Wojtsekhowski, and G. D. Cates. Gas dynamics in high-luminosity polarized ^{3}he targets using diffusion and convection. *Phys. Rev. C*, 84:065201, Dec 2011.

[27] W. A. Fitzsimmons, L. L. Tankersley, and G. K. Walters. Nature of surface-induced nuclear-spin relaxation of gaseous he^3. *Phys. Rev.*, 179:156–165, Mar 1969.

[28] J. Frenkel. *Kinetic Theory of Liquids*.

[29] R. L. Gamblin and T. R. Carver. Polarization and relaxation processes in he^3 gas. *Phys. Rev.*, 138:A946–A960, May 1965.

[30] L. E. Glass. *http://www.larsonelectronicglass.com*.

[31] W. Happer, G. Cates, M. Romalis, and C. Erickson. U.s. patent no. 6318092. 2001.

[32] W. Heil, H. Humblot, E. Otten, M. Schafer, R. Sarkau, and M. Leduc. Very long nuclear relaxation times of spin-polarized ^{3}he in metal coated cells. *Phys. Rev. A*, 201:337–343, May 1995.

[33] W. G. Houskeeper. The art of sealing base metals through glass. *Transactions of the American Institute of Electrical Engineers*, XLII:870–877, 1923.

[34] M. F. Hsu, G. D. Cates, I. Kominis, I. A. Aksay, and D. M. Dabbs. Sol-gel coated glass cells for spin-exchange polarized 3he. *Applied Physics Letters*, 77(13):2069–2071, 2000.

[35] E. T. Inc. *http://www.epner.com*.

[36] B. Larson, O. Hausser, P. P. J. Delheij, D. M. Whittal, and D. Thiessen. Optical pumping of rb in the presence of high-pressure ^{3}He buffer gas. *Phys. Rev. A*, 44:3108–3118, Sep 1991.

[37] D. Matyas. Characterizing ^{3}he nuclear spin relaxation in vessels of glass and metal. *Master thesis, University of Virginia*, 2016.

[38] E. Merzbacher. *Quantum Mechanics*. 1998.

[39] N. R. Newbury, A. S. Barton, P. Bogorad, G. D. Cates, M. Gatzke, B. Saam, L. Han, R. Holmes, P. A. Souder, J. Xu, and D. Benton. Laser polarized muonic helium. *Phys. Rev. Lett.*, 67:3219–3222, Dec 1991.

[40] X. Qian, K. Allada, C. Dutta, J. Huang, J. Katich, Y. Wang, Y. Zhang, K. Aniol, J. R. M. Annand, T. Averett, F. Benmokhtar, W. Bertozzi, P. C. Bradshaw, P. Bosted, A. Camsonne, M. Canan, G. D. Cates, C. Chen, J.-P. Chen, W. Chen, K. Chirapatpimol, E. Chudakov, E. Cisbani, J. C. Cornejo, F. Cusanno, M. M. Dalton, W. Deconinck, C. W. de Jager, R. De Leo, X. Deng, A. Deur, H. Ding, P. A. M. Dolph, D. Dutta, L. El Fassi, S. Frullani, H. Gao, F. Garibaldi, D. Gaskell, S. Gilad, R. Gilman, O. Glamazdin, S. Golge, L. Guo, D. Hamilton, O. Hansen, D. W. Higinbotham, T. Holmstrom, M. Huang, H. F. Ibrahim, M. Iodice, X. Jiang, G. Jin, M. K. Jones, A. Kelleher, W. Kim, A. Kolarkar, W. Korsch, J. J. LeRose, X. Li, Y. Li, R. Lindgren, N. Liyanage, E. Long, H.-J. Lu, D. J. Margaziotis, P. Markowitz, S. Marrone, D. McNulty, Z.-E. Meziani, R. Michaels, B. Moffit, C. Muñoz Camacho, S. Nanda, A. Narayan, V. Nelyubin,

B. Norum, Y. Oh, M. Osipenko, D. Parno, J. C. Peng, S. K. Phillips, M. Posik, A. J. R. Puckett, Y. Qiang, A. Rakhman, R. D. Ransome, S. Riordan, A. Saha, B. Sawatzky, E. Schulte, A. Shahinyan, M. H. Shabestari, S. Širca, S. Stepanyan, R. Subedi, V. Sulkosky, L.-G. Tang, A. Tobias, G. M. Urciuoli, I. Vilardi, K. Wang, B. Wojtsekhowski, X. Yan, H. Yao, Y. Ye, Z. Ye, L. Yuan, X. Zhan, Y.-W. Zhang, B. Zhao, X. Zheng, L. Zhu, X. Zhu, and X. Zong. Single spin asymmetries in charged pion production from semi-inclusive deep inelastic scattering on a transversely polarized ^{3}He target at $Q^2 = 1.4\breve{}2.7$ gev^2. *Phys. Rev. Lett.*, 107:072003, Aug 2011.

[41] I. I. Rabi, N. F. Ramsey, and J. Schwinger. Use of rotating coordinates in magnetic resonance problems. *Rev. Mod. Phys.*, 26:167–171, Apr 1954.

[42] M. L. R.Barbe and F. Laloe. Experimental verifications - measurement of the he3 self-diffusion coefficient. 35:935–951, 1974.

[43] S. Riordan, S. Abrahamyan, B. Craver, A. Kelleher, A. Kolarkar, J. Miller, G. D. Cates, N. Liyanage, B. Wojtsekhowski, A. Acha, K. Allada, B. Anderson, K. A. Aniol, J. R. M. Annand, J. Arrington, T. Averett, A. Beck, M. Bellis, W. Boeglin, H. Breuer, J. R. Calarco, A. Camsonne, J. P. Chen, E. Chudakov, L. Coman, B. Crowe, F. Cusanno, D. Day, P. Degtyarenko, P. A. M. Dolph, C. Dutta, C. Ferdi, C. Fernández-Ramírez, R. Feuerbach, L. M. Fraile, G. Franklin, S. Frullani, S. Fuchs, F. Garibaldi, N. Gevorgyan, R. Gilman, A. Glamazdin, J. Gomez, K. Grimm, J.-O. Hansen, J. L. Herraiz, D. W. Higinbotham, R. Holmes, T. Holmstrom, D. Howell, C. W. de Jager, X. Jiang, M. K. Jones, J. Katich, L. J. Kaufman, M. Khandaker, J. J. Kelly, D. Kiselev, W. Ko-

rsch, J. LeRose, R. Lindgren, P. Markowitz, D. J. Margaziotis, S. M.-T. Beck, S. Mayilyan, K. McCormick, Z.-E. Meziani, R. Michaels, B. Moffit, S. Nanda, V. Nelyubin, T. Ngo, D. M. Nikolenko, B. Norum, L. Pentchev, C. F. Perdrisat, E. Piasetzky, R. Pomatsalyuk, D. Protopopescu, A. J. R. Puckett, V. A. Punjabi, X. Qian, Y. Qiang, B. Quinn, I. Rachek, R. D. Ransome, P. E. Reimer, B. Reitz, J. Roche, G. Ron, O. Rondon, G. Rosner, A. Saha, M. M. Sargsian, B. Sawatzky, J. Segal, M. Shabestari, A. Shahinyan, Y. Shestakov, J. Singh, S. Širca, P. Souder, S. Stepanyan, V. Stibunov, V. Sulkosky, S. Tajima, W. A. Tobias, J. M. Udias, G. M. Urciuoli, B. Vlahovic, H. Voskanyan, K. Wang, F. R. Wesselmann, J. R. Vignote, S. A. Wood, J. Wright, H. Yao, and X. Zhu. Measurements of the electric form factor of the neutron up to $Q^2 = 3.4$ gev^2 using the reaction $^3\vec{\text{he}}(\vec{e}, e'n)pp$. *Phys. Rev. Lett.*, 105:262302, Dec 2010.

[44] M. V. Romalis and G. D. Cates. Accurate ^{3}He polarimetry using the rb zeeman frequency shift due to the Rb$-^3$He spin-exchange collisions. *Phys. Rev. A*, 58:3004–3011, Oct 1998.

[45] M. V. Romalis, E. Miron, and G. D. Cates. Pressure broadening of rb d_1 and d_2 lines by ^{3}he, ^{4}he, n_2, and xe: line cores and near wings. *Phys. Rev. A*, 56(6), 1997.

[46] L. D. Schearer, F. D. Colegrove, and G. K. Walters. Large he^3 nuclear polarization. *Phys. Rev. Lett.*, 10:108–110, Feb 1963.

[47] L. D. Schearer and G. K. Walters. Nuclear spin-lattice relaxation in the presence of magnetic-field gradients. *Phys. Rev.*, 139:A1398–A1402, Aug 1965.

[48] J. Schmiedeskamp, W. Heil, W. E. Otten, K. R. Kremer, A. Simon, and J. Zimmer. Paramagnetic relaxation of spin polarized 3he at bare glass surfaces. *The European Physical Journal D - Atomic, Molecular, Optical and Plasma Physics*, 38(3):427–438, 2006.

[49] J. T. Singh, P. A. M. Dolph, W. A. Tobias, T. D. Averett, A. Kelleher, K. E. Mooney, V. V. Nelyubin, Y. Wang, Y. Zheng, and G. D. Cates. Development of high-performance alkali-hybrid polarized ^{3}He targets for electron scattering. *Phys. Rev. C*, 91:055205, May 2015.

[50] C. P. Slichter. *Principles of Magnetic Resonance*.

[51] W. Smythe. *Static and Dynamic Electricity*.

[52] A. E. A. M. I. Technologies. *http://www.ableelectropolishing.com*.

[53] M. Wagshul and T. Chupp. Optical pumping of high-density rb with a broadband dye laser and gaalas diode laser arrays: Application to ^{3}he polarization. *Phys. Rev. A.*, 40, 1989.

[54] M. Wagshul and T. Chupp. Laser optical pumping of high-density rb in polarized ^{3}he targets. *Phys. Rev. A*, 49:3854–3869, 1994.

[55] T. G. Walker and W. Happer. Spin-exchange optical pumping of noble-gas nuclei. *Rev. Mod. Phys.*, 69:629–642, Apr 1997.

[56] Y. Zheng. Low field mri and the development of polarized nuclear imaging (pni)-a new imaging modality, 2015.

Appendix A

Appendix title

This is Appendix A.

You can have additional appendices too (*e.g.*, `apdxb.tex`, `apdxc.tex`, *etc.*). If you don't need any appendices, delete the appendix related lines from `thesis.tex` and the file names from `Makefile`.